

On the ferromagnetic structure of the intermetallic borocarbide

TbCo₂B₂C

M. ElMassalami, R. Moreno, R. M. Saeed, F. A. B. Chaves, C. M. Chaves

*Instituto de Fisica, Universidade Federal do Rio de Janeiro,
Caixa Postal 68528, 21945-970 Rio de Janeiro, Brazil*

H. Takeya

*National Institute for Materials Science,
1-2-1 Sengen, Tsukuba, Ibaraki 305-0047, Japan*

B. Ouladdiaf

Institut Laue-Langevin, B.P.156 ,38042 Grenoble Cedex 9, France

M. Amara

Institut Néel - CNRS, Bât. D, B.P. 166, 38042 Grenoble Cedex 9, France

(Dated: October 30, 2018)

Abstract

Based on magnetization, specific heat, magnetostriction, and neutron diffraction studies on single-crystal TbCo₂B₂C, it is found out that the paramagnetic properties, down to liquid nitrogen temperatures, are well described by a Curie-Weiss behavior of the Tb³⁺ moments. Furthermore, below $T_c = 6.3$ K, the Tb-sublattice undergoes a ferromagnetic (FM) phase transition with the easy axis being along the (100) direction and, concomitantly, the unit cell undergoes a tetragonal-to-orthorhombic distortion. For fields up to 90 kOe, no field-induced splitting of the Co 3d orbitals was observed; as such the internal field must be well below the critical value needed to polarize the Co 3d subsystem. The manifestation of a FM state in TbCo₂B₂C is unique among all other isomorphous borocarbides, in particular TbNi₂B₂C ($T_N = 15$ K, incommensurate modulated magnetic state) even though the Tb-ions in both isomorphs have almost the same crystalline electric field properties. The difference in the magnetic modes of these Tb-based isomorphs is attributed to a difference in their exchange couplings caused by a variation in their lattice parameters and in the position of their Fermi levels.

I. INTRODUCTION

Whenever a family of compounds, containing $3d$ transition-metal (M) and rare-earth (R) atoms, manifests similar band structures, the trend in their magnetic properties can be rationalized in terms of the position of the Fermi level E_F within the density of states $N(E)$ curve. The cubic, Laves-type RM_2 family of compounds provides a best illustration.^{1,2,3,4} Here, it is commonly considered that the R -ion moments are localized while the M moments, if they exist, are itinerant. Assuming further that the mutual interactions among the magnetic ions can be described within the molecular field theory and, in addition, using Landau phase-transition arguments together with Stoner and Wohlfarth-Rhodes criteria, then the magnetic properties of the whole RM_2 family can be classified according to the first few energy derivatives of $N(E)$ evaluated at E_F .^{1,2,3,4} This model is successful in explaining the evolution of the paramagnetic susceptibility, the type of the magnetic phase transition, the relative magnitude of the critical temperature, and, moreover, the magnetism of the $3d$ subsystem; in particular it explains why the Ni sublattice is magnetically silent in RNi_2 while the Co subsystem has an intermediate character: being strongly exchange-enhanced in RCo_2 ($R = Y, Lu$) while developing a delocalized moment in magnetic RCo_2 . For such RCo_2 series, it was found out that an adequate effective magnetic field at the Co site, $H_{\text{eff}}^{\text{Co}}$, is able, at and above a critical field $H_{\text{cr}}^{\text{Co}}$, to induce a metamagnetic transition due to which the Co atom acquires an itinerant moment of $\sim 1\mu_B$.

The above-mentioned interplay between the magnetism of M and R subsystems is expected to be manifested also in the quaternary borocarbides RM_2B_2C family (see e.g. Ref. 5 and references therein). Though the investigation of this interplay is of interest for the understanding of the magnetism (and superconductivity) of this family, there are only very few studies bearing on this subject and these are mostly limited to the RNi_2B_2C series. Nevertheless, the extensive magnetic characterization of this RNi_2B_2C series did clarify the influence of R (M) on their overall magnetic (superconducting) properties;⁵ in particular, it is established that while the M -doping hardly influences the magnetic properties (but leads invariably to a degradation of the superconductivity), the variation in R strongly modifies the magnetic structure: for $R = Pr, Ho, Dy$, the magnetic structures consist of a commensurate antiferromagnetic, AFM, state,^{6,7,8} that of $R = Tm$ is incommensurate modulated structure with $\vec{q} \simeq (0.093, 0.093, 0)$,^{6,9,10} and those of $R = Er, Tb, Gd$ are incommensurate modulated

states with $\vec{q} \simeq (0.55, 0, 0)$.^{6,11,12,13,14} At T_{WF} (which is $< T_{\text{N}}$), each of the latter states transforms into an equal-amplitude, squared-up state and in the particular cases of $R = \text{Er}$ and Tb , this transformation leads to a surge of a weak ferromagnetic component.^{15,16,17,18} It is an experimental fact that none of the Ni-based compounds manifests a ferromagnetic, FM, ground state though there is, at least for $R = \text{Pr}, \text{Ho}, \text{Dy}$, a strong FM intralayer coupling.

It is recalled that the Ni subsystem in $\text{YNi}_2\text{B}_2\text{C}$ is magnetically inactive⁵ while the Co subsystem in $\text{YCo}_2\text{B}_2\text{C}$ manifests an exchange enhanced paramagnetism.¹⁹ based on the above model, these features indicate that E_F in the Ni-based compound is above a filled $3d$ band and, in addition, is not at a steep region of $N(E)$ while for the Co-based compound the curvature of $N(E)$ at E_F must be positive and nonnegligible. Indeed electronic structure calculations^{20,21,22,23} on $R\text{Ni}_2\text{B}_2\text{C}$ ($R = \text{Lu}, \text{Y}$) showed that E_F is situated at the top of a pronounced and narrow $N(E)$ peak and this peak lies on the top edge of nearly filled Ni($3d$) bands: this, together with the intermediate electron-phonon coupling and the smaller Stoner factor, explains the surge of the superconductivity as well as the nonmagnetic character of the Ni-sublattice. Furthermore, in case of a FM order, such an $N(E)$ peak at E_F would be exchange split due to the direct intra-atomic $4f$ - $5d$ exchange interaction:²⁰ such a split would be higher than the superconducting gap; it is an experimental fact that, due to their AFM structures, none of the magnetic $R\text{Ni}_2\text{B}_2\text{C}$ superconductors shows this splitting.

Band structure calculations²⁰ on $\text{LuCo}_2\text{B}_2\text{C}$ showed that, for such isomorphous borocarbides, the rigid band model yields a reasonable description of the band filling. Furthermore, E_F is situated at the decreasing but right-hand side of one of the peaks that receives a considerable contribution from the Co $3d$ -band, and that $N(E_F)$ is of the same magnitude as that of $\text{LuNi}_2\text{B}_2\text{C}$: the latter finding is consistent with the observation that the Sommerfeld linear specific heat coefficients of $\text{YCo}_2\text{B}_2\text{C}$ and $\text{YNi}_2\text{B}_2\text{C}$ are equal.²⁴ Furthermore, as that the first derivatives of $N(E)$ are nonnegligible, then we expect the Co sublattice, similar to $R\text{Co}_2$, to develop an intermediate character (or even to be polarized) if $H_{\text{eff}}^{\text{Co}} > H_{\text{cr}}^{\text{Co}}$: the intermediate character is indeed observed in $\text{YCo}_2\text{B}_2\text{C}$;^{19,25} the possibility of Co-subsystem polarization, on the other hand, would be addressed in this work. As far as the R -sublattice magnetism is concerned, it is expected that the difference in the lattice parameters and in the electronic band structure of the Co- and Ni-based borocarbides would imply a modification in the character of the mediating RKKY-type interactions and consequently in the character of their magnetic ground states.

In this paper, we report on the extensive magnetic characterization of $\text{TbCo}_2\text{B}_2\text{C}$. The successful synthesis of a single-crystal sample of $\text{TbCo}_2\text{B}_2\text{C}$ made it possible to identify unambiguously the paramagnetic as well as the ordered-state properties of the Tb sublattice: the former is dominated by a Curie-Weiss behavior while the latter is found to be a FM structure with the easy axis lying along the a direction. Such a FM state is in sharp contrast to the AFM-type mode of the isomorphous $\text{TbNi}_2\text{B}_2\text{C}$.^{13,16,26,27,28,29} This work also addressed the question of whether the surge of this FM state (with a strong Tb moment and consequently a strong $H_{\text{eff}}^{\text{Co}}$) is able to polarize the Co $3d$ subsystem. Our results suggest that in spite of the intermediate character of the Co $3d$ subsystem, the induced $H_{\text{eff}}^{\text{Co}}$ is not able to bring about an unambiguous spontaneous polarization.

II. EXPERIMENT

99.5% ^{11}B enriched polycrystals of $\text{TbCo}_2\text{B}_2\text{C}$ were prepared by conventional arc-melt method. These polycrystals were used as feeding rods during a floating-zone synthesis, a process that we used for single crystals growth.³⁰

Characterization were carried out using magnetization [$M(T, H)$, extraction method within the ranges $1.9 \leq T \leq 300$ K and $H \leq 90$ kOe] and zero-field specific heat [$C(T)$, semi-adiabatic method within the range $0.5 \leq T \leq 15$ K, accuracy better than 4%]. A high-accuracy capacitance dilatometer³¹ was used for measuring the thermal expansion or forced magnetostriction with a resolution better than 1 Å. The relative change in length, measured along the cosine directions $(\beta_1\beta_2\beta_3)$ when a field is applied along the cosine direction (xyz) , is denoted as $^{\beta_1\beta_2\beta_3}\lambda_{xyz}(T) = [l(T, H) - l_0(T_0, H_0)] / l_0(T_0, H_0)$.

Neutron-diffraction measurements were carried out at the Institut Laue-Langevin in Grenoble, France. Measurements were carried out on a powdered as-prepared arc-melt polycrystalline sample (since large quantity is desirable, see § III.D below) as well as on a single crystal sample. The powder diffraction patterns were collected within a temperature range 2 to 40 K using the D1B diffractometer with a selected incident wavelength of 2.42 Å; Rietveld refinements of both crystallographic and magnetic structures were carried out using the FULLPROF package of Rodriguez-Carvajal (www.ill.fr/dif/Soft/fp). Single crystal diffraction studies were performed on the D10 four-circle diffractometer with $\lambda = 2.3606$ Å over a wide range of q space and within the temperature range $1.7 < T < 8\text{K}$.

III. RESULTS

A. Magnetization

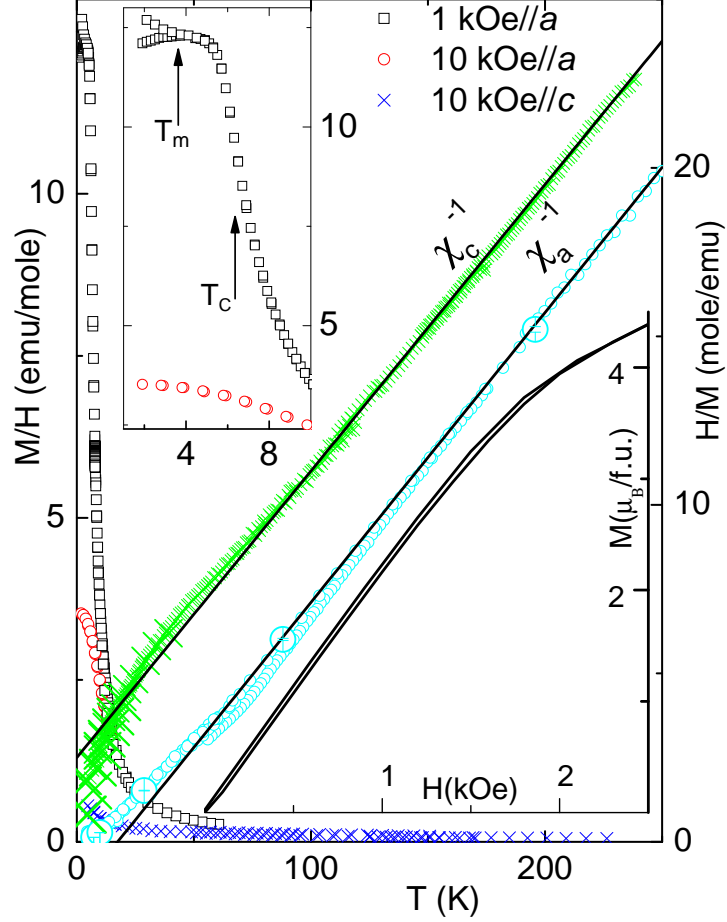


FIG. 1: (Color online) T -dependent χ_{dc} (left-hand ordinate) and χ_{dc}^{-1} (right-hand ordinate) curves of $\text{TbCo}_2\text{B}_2\text{C}$ measured along the a and c axes. The solid lines represent $\chi = C/(T - \theta)$; C and θ are the Curie-Weiss constants. The large symbols on the $\chi_{dc}^{-1}(T)$ curves represent the $H/M(T, H \rightarrow 0)$ as obtained from the Arrot plot. The upper-left inset shows, on expanded scales, the low-temperature $\chi_{dc}(T, H//a)$ for $H = 1$ kOe and 10 kOe. The lower-right inset shows the magnetization isotherms at $T=1.9$ K which demonstrates that for $H \geq 2$ kOe, there is no hysteresis effect (see text).

Figure 1 shows the T -dependent χ_{dc} and χ_{dc}^{-1} curves that were measured at different fields and along the two principal tetragonal axes. The large symbols on the $\chi_{dc}^{-1}(T)$ curve represent

the $H/M(T, H \rightarrow 0)$ obtained from the Arrot plot: the excellent agreement emphasizes that, within this temperature range, the contribution of magnetic impurities is negligible. A Curie-Weiss fit down to liquid-nitrogen temperatures of $\chi_{dc}(T, H||c)$ gives $\mu_{\text{eff}} = 9.7(1)\mu_{\text{B}}$ and $\theta_c = -29.4(1)$ K while that of $\chi_{dc}(T, H||a)$ gives $\mu_{\text{eff}} = 9.6(1)\mu_{\text{B}}$ and $\theta_a = 14.4(1)$ K. Evidently, there are anisotropic forces but the effective moments are in excellent agreement with the value expected for a free Tb^{3+} ion. Based on these anisotropic θ values, the first Stevens coefficient in the crystal field description of a tetragonal symmetry is estimated to be $B_2^0 = 0.88(2)$ K; this compares well in sign and magnitude with that of $\text{TbNi}_2\text{B}_2\text{C}$ ($B_2^0 = 1.2(1)$ K).³¹ This similarity suggests that the crystalline electric field, CEF, at the Tb^{3+} site of both isomorphs are similar: indeed both sites have the same D_{4h} symmetry and almost the same charge distribution. On lowering the temperatures toward liquid helium region, $\chi_{dc}(T, H||a)$ increases relatively fast and afterward tends toward saturation. Considering the characteristic magnetic features manifested in the magnetization, specific heat, and neutron diffraction (see below), this fast increase (which is followed by saturation) is caused by the process of approaching and the eventual onset of a FM order wherein the moments point along the a axis: $T_C = 6.3(2)$ K is the point of maximum inclination.

The upper-left inset of Fig. 1 shows, on an expanded scale, a magnetic hysteresis occurring at $T \leq T_m = 3.7(2)$ K and $H = 1$ kOe. The $M(H||a, 1.9$ K) curve, shown in the lower-right inset of Fig. 1, reveals that this hysteresis effect disappears for $H \geq 2$ kOe. Since this T_m -feature is sample-dependent (see below), it is attributed to a contaminating magnetic phase, the magnetization of which saturates completely to $0.05 \mu_{\text{B}}$ /formula unit for field higher than 2 kOe. Based on the weight ratios of the magnetic moments, the fraction of the Tb ions in this spurious phase relative to the major $\text{TbCo}_2\text{B}_2\text{C}$ phase is estimated to be 0.7%.

Figure 2 confirms the above-mentioned magnetic anisotropy, due to which the a (c) is the easy (hard) axis. Within the studied ranges of H and T , the magnetization isotherms do not show any field-induced transition, rather, only a monotonic and steady increase (tending towards saturation) which is characteristic of a forced domain alignment: this supports the earlier inference of a FM order. Furthermore, the high-field magnetization increases as $M(H||a, 2\text{K}) = \mu_{\text{sp}} + \chi_{\text{hf}}H$ [$\mu_{\text{sp}} = 7.6(3)\mu_{\text{B}}$, $\chi_{\text{hf}} = 6.8(4) \times 10^{-6} \mu_{\text{B}}/\text{Oe}$ corresponding to $38(2) \times 10^{-3}$ emu/mol] attaining $\mu(90 \text{ kOe}, 2 \text{ K}) = 8.2\mu_{\text{B}}$. μ_{sp} is only 3% lower than the reported moment of $\text{TbNi}_2\text{B}_2\text{C}$ ($\mu_{\text{Tb}} = 7.78 \mu_{\text{B}}$,^{6,26}) but 16% lower than the one expected

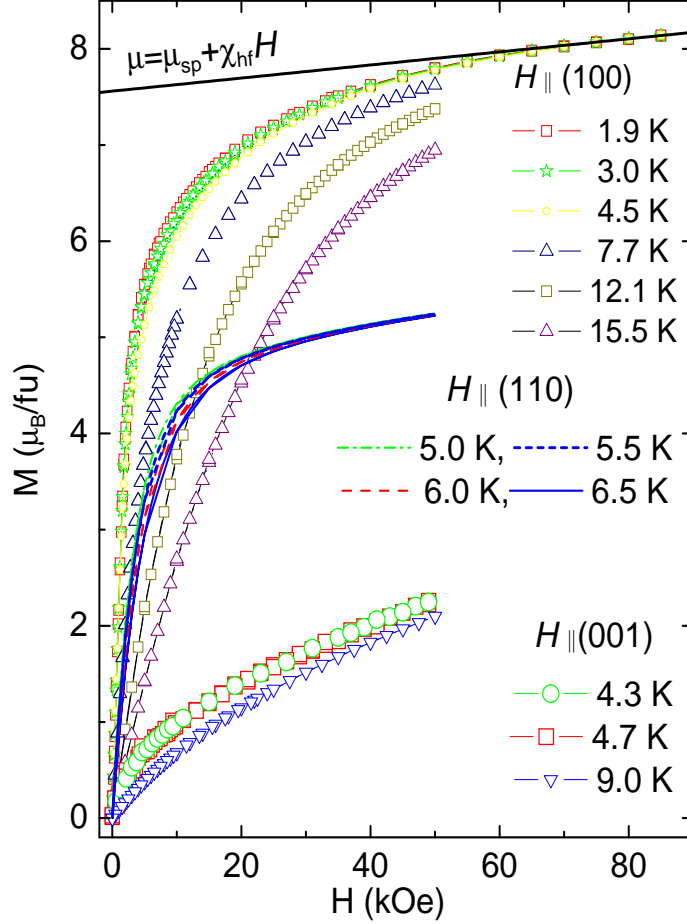


FIG. 2: (Color online) Magnetization isotherms of $\text{TbCo}_2\text{B}_2\text{C}$ at different temperatures and for different field orientations. Two different set-ups were employed one with a field up to 90 kOe and another up to 50 kOe. The high-field magnetization evolves as $M(H \parallel a, 2\text{K}) = \mu_{\text{sp}} + \chi_{\text{hf}}H$ and is represented by the solid line (see text).

for a free Tb^{3+} ion: this observed moment lowering confirms the above-mentioned influence of the CEF effects and that these effects are similar to the ones observed in the Ni-based isomorph. Alternatively, let us assume that the difference between μ_{sp} of $\text{TbCo}_2\text{B}_2\text{C}$ and the reported moment of $\text{TbNi}_2\text{B}_2\text{C}$ is due exclusively to the spontaneous polarization of the Co $3d$ orbitals which are coupled ferrimagnetically to the FM Tb sublattice. Then, based on the relation $\mu_{\text{sp}}(\text{TbCo}_2\text{B}_2\text{C}) = \mu_{\text{sp}}(\text{TbNi}_2\text{B}_2\text{C}) - 2\mu_{\text{Co}}$, the maximum possible Co moment would be $\mu_{\text{Co}} = 0.25 \mu_{\text{B}}$. Such a μ_{Co} value is surprisingly small, amounting to only 0.25 hole/Co atom in the $3d$ band; this value is almost one fourth of the Co moment encountered in the heavy members of the $R\text{Co}_2$ series,³ but it is similar to the value observed in the low

spin state of Co in, e.g., ErCo_2 .^{32,33} It is more likely that $H_{\text{eff}}^{\text{Co}} < H_{\text{cr}}^{\text{Co}}$ (see § IV) since if there is any spontaneous Co polarization then the induced moment should be much higher than $0.25 \mu_B$. As the CW law describes well the paramagnetic susceptibility of $\text{TbCo}_2\text{B}_2\text{C}$ (see above), then the exchange-enhancement factor for the Co-subsystem susceptibility must be extremely small.

B. Specific heat

Figure 3 shows the zero-field magnetic specific heat and entropy of single-crystal $\text{TbCo}_2\text{B}_2\text{C}$ obtained after subtracting the nuclear, electronic, and lattice contributions (the latter two were obtained from $\text{YCo}_2\text{B}_2\text{C}$).^{19,24} The nuclear contribution is of dominant importance only at very low temperatures and was evaluated from the diagonalization of the hyperfine Hamiltonian.³⁴ It is worth mentioning that at very low-temperature, the nuclear contribution is much stronger than the magnetic one: as such the propagation of errors due to successive subtraction of non-magnon contributions would eventually influence the absolute value of $C_M(T)$; this may undermine the quality of the comparison between the theoretical and experimental magnon contributions (see Fig. 3).

Both $C_{\text{mag}}(T)$ and $S_{\text{mag}}(T)$ curves do confirm the onset of the magnetic order at T_c : the former curve rises very sharply at T_c while the latter manifests a pronounced change of slope. Considering the magnetic structure to be associated with the FM order of the Tb-sublattice (see below), we fit the experimental $C_{\text{mag}}(T)$ to the theoretical magnon expression of Eq. A5 (see Appendix): as can be seen in Fig. 3, the excellent fit to Eq. A5 gives the spin-wave stiffness coefficient $D=26.3(5)$ K and the gap parameter $\Delta=8.4(2)$ K. The high value of D is indicative of stronger effective exchange couplings. On the other hand, the value of Δ (which from Eq. A3 is a measure of the anisotropic field) is consistent with the strong anisotropic features observed in the magnetization measurements.

The inset of Fig. 3 compares the measured $C_{\text{mag}}(T)$ of a single-crystal sample with that of a polycrystalline one. Evidently the T_m -transition is sample-dependent: while $C_{\text{mag}}(T)$ of the polycrystalline sample manifests a pronounced event at $T_m=3.6(2)$ K, that of the single-crystal hardly shows any anomaly. As mentioned above, the single-crystal sample contains only a 0.7% spurious phase and this concentration limit is lower than the resolution of the specific heat set-up.

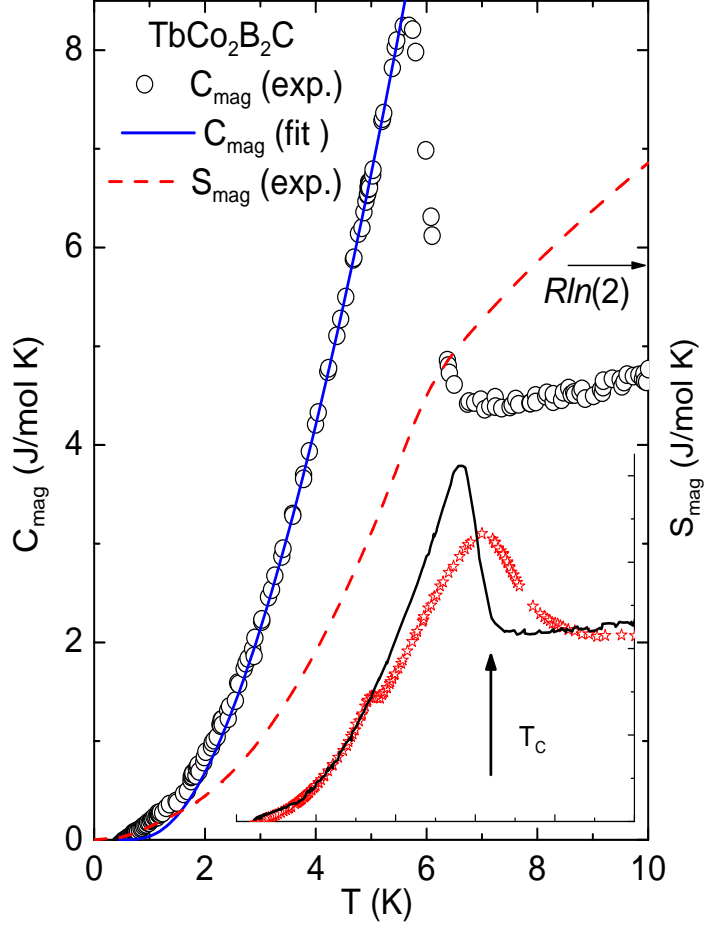


FIG. 3: (Color online) Zero-field magnetic specific heat (symbol) and calculated magnetic entropy (dashed line) of single-crystal $\text{TbCo}_2\text{B}_2\text{C}$. The nuclear, electronic, and lattice contributions were already subtracted (the latter two were obtained from $\text{YCo}_2\text{B}_2\text{C}$).^{19,24} The solid line represents a fit to the expression of the magnon contribution (Eq. A5) assuming a FM order of the Tb sublattice. The inset (with the same scales as the main panel) compares the single-crystal magnetic specific heat (solid line) with that of a polycrystalline sample (symbol); the observed difference reflects a strong dependence on the sample form, contamination, and history. Nevertheless, their magnetic entropies approach each other for $T > T_c$ confirming, as it should, the conservation of the total entropy (see text).

C. magnetostriction

Figure 4 shows the forced magnetostriction isotherms measured along the a and b axis with $H \parallel a$. Once more (apart from the low-field, domain-wall sweeping-out region and the

saturated regime) there is no metamagnetic transition in these isotherms. The inset of Fig. 4 indicates clearly that below T_c , $\text{TbCo}_2\text{B}_2\text{C}$ undergoes a spontaneous distortion which - based on Fig. 4(a), see also § III.D - is attributed to an orthorhombic distortion of the tetragonal unit cell. A similar distortion was reported for $\text{TbNi}_2\text{B}_2\text{C}$.^{16,29,31,35,36} Then the behavior of the forced magnetostriction of Fig.4 can be understood as follows: at zero-field, there is an equal distribution of domains along each of the a and b axes; an applied field along, say, the a axis would involve a rearrangement of the orthorhombically-distorted domains and as such induces an increase in $M(H||a)$ [Fig. 4 (b)], an increase in $^{100}\lambda_{100}(H)$, and a decrease in $^{010}\lambda_{100}(H)$ [Fig. 4 (a)].

D. Neutron Diffraction

The thermal evolution of the powder diffractograms are shown Figs. 5-6. For $T > T_c$, the patterns consist of the tetragonal crystal structure of $\text{TbCo}_2\text{B}_2\text{C}$ and a small impurity phase. On the other hand, for $T_m < T < T_c$, it is evident that the magnetic reflections are piled up on the top of the nuclear Bragg peaks: a $q_0=(000)$ mode. Considering that the paramagnetic state is dominated by the Tb moment, that the evolution of the isothermal magnetization and magnetostriction indicates no metamagnetic transition which can be related to the onset of Co moment, then this q_0 mode must be related to the Tb sublattice. Furthermore, since the Tb ion occupies the special $2a$ site in the unit cell, then this mode must be FM: confirming the conclusions drawn from the magnetization, magnetostriction, and specific heat studies. Indeed, Fig. 6 (a) confirms that this pattern is a FM mode. Alternatively, if this mode is related to the Co sublattice then, due to the multiplicity of the $4d$ site occupied by the Co atoms, the magnetic order should be either AFM (if only due to Co subsystem) or ferrimagnetic (if both subsystems are ordered): in the light of all the above-mentioned results, both possibilities must be ruled out (see also § IV).

To extract more information, Rietveld analysis was carried out on the diffractograms measured within the range $T_m < T < T_c$. Because of the structural distortion, we used the $Immm$ space group together with the parameters given in Table I. Representative analyzed diffractograms are shown in Fig. 7 while the obtained cell parameters and the magnetic moment are given in Fig. 8. The analysis indicates that the lattice parameters [Fig. 8 (a-b)] undergoes a noticeable orthorhombic distortion below T_c which is consistent with

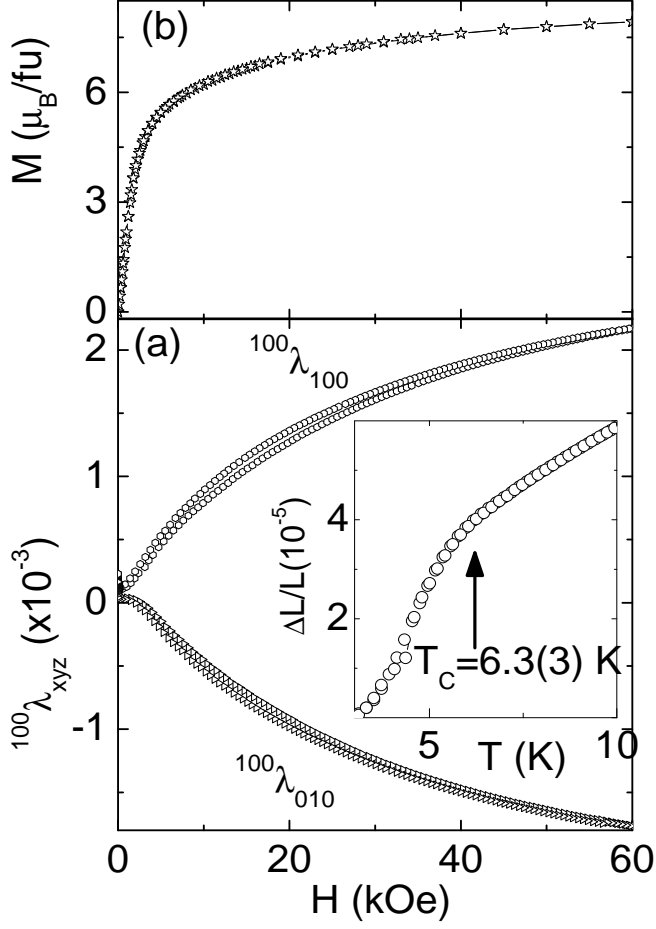


FIG. 4: Representative forced magnetostrictions (a) $^{100}\lambda_{100}(H, 3\text{K})$ and $^{100}\lambda_{010}(H, 3\text{K})$ curves of $\text{TbCo}_2\text{B}_2\text{C}$ are compared to (b) the isothermal magnetization at 3 K. The magnetostriction curves are given relative to their zero-field values. The inset shows the thermal evolution of the zero-field $\Delta L/L$ measured along the a axis. The arrow marks the T_c value which was determined from the specific heat measurement of Fig.3.

the magnetoelastic effects observed in Fig. 4. Furthermore, the analysis revealed that the zero-field Tb magnetic moment is along the longest side of the base of the orthorhombic cell.

Below $T_m \approx 3.7$ K, the thermal evolution of the diffractograms reveals two features [Figs. 6 (b and c)]: First, the intensity of the FM mode evolves smoothly and independently. Secondly, there is a surge of additional magnetic peaks [marked by the vertical arrows in the difference plots of Fig. 6 (b and c)]. Since Figs. 1 to 4 do not indicate any event that can be related to an order-to-order transition of Tb magnetic order, then these peaks can not be associated with the magnetic pattern of the Tb-sublattice. As these diffractograms

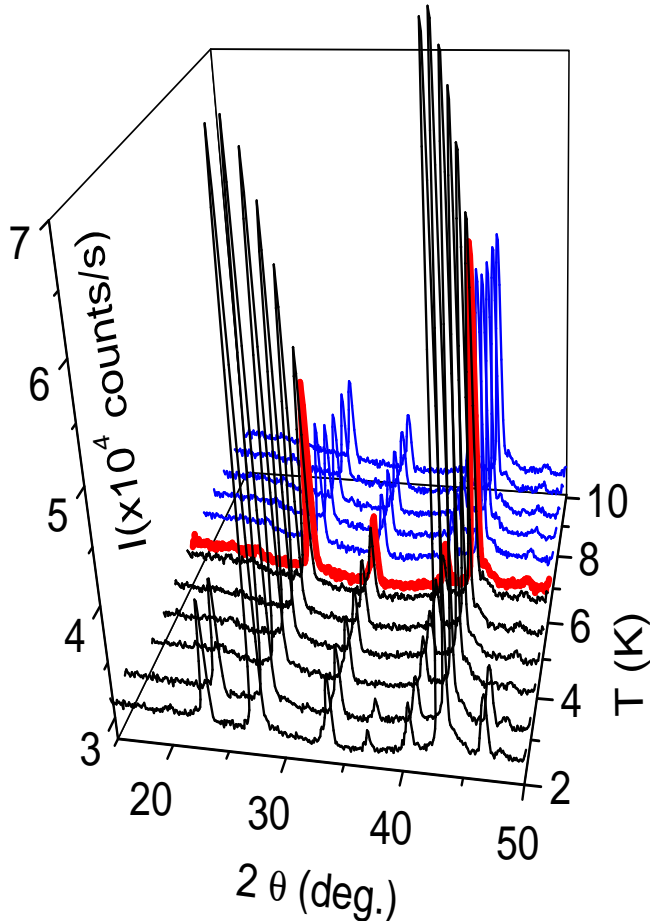


FIG. 5: (Color online) Representative neutron powder diffractograms of as-prepared polycrystalline $\text{TbCo}_2\text{B}_2\text{C}$. To aid in visualizing the magnetic modes, this plot is limited to temperatures below 10 K and to scattering angle lower than 50° . The diffractogram at 6.4 K (denoted by thick solid line) can be taken as a demarcation between the paramagnetic and FM phases.

were collected on as-prepared, arc-melt polycrystalline sample - which as mentioned above contains magnetic contamination - then these additional peaks are taken to be due to the same magnetic contamination, which is responsible for the hysteresis event in Fig. 1 and the weak specific heat anomaly in the inset of Fig. 3 (we argue, in § IV, that these events can not be due to an onset of a Co itinerant moment).

Various q -scans within the range $1.7 < T < 8$ K were performed on a single crystal of $\text{TbCo}_2\text{B}_2\text{C}$. A wide range of q space were scanned while maintaining the temperature constant at 1.7 K. Indeed, most of the nuclear (and ferromagnetic) peaks that satisfy the relation $h + k + l = 2n$ were observed. In addition, we also looked, at 1.7 K, for any modulated

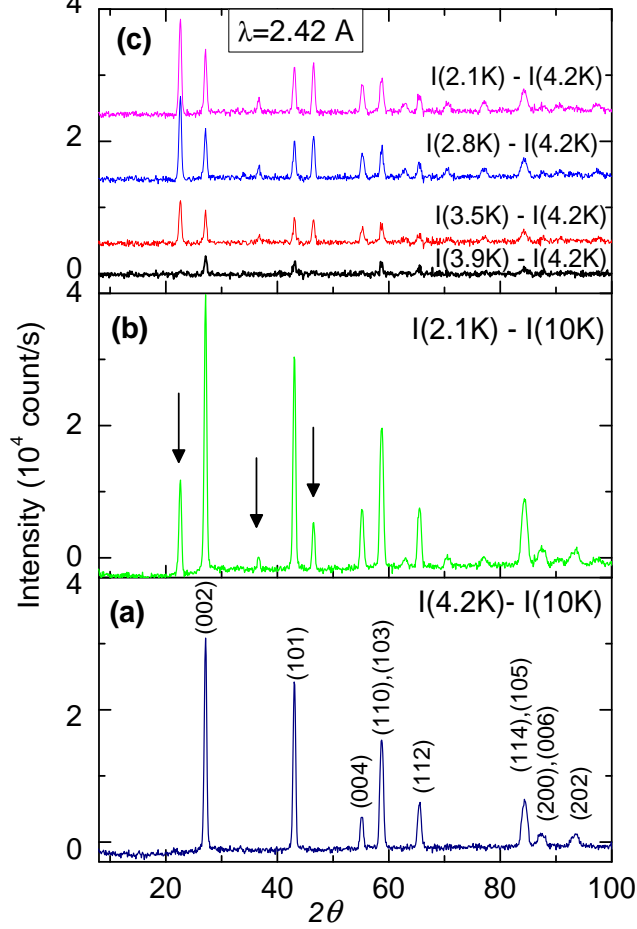


FIG. 6: (Color online) The magnetic diffractograms of as-prepared polycrystalline $\text{TbCo}_2\text{B}_2\text{C}$ sample. These were obtained after subtracting either the pattern at 10 K (a and b) or the pattern at 4.2 K (c). (a) The FM mode; (b) the superposition of the FM and the magnetic contamination contribution at $T=2.0$ K (the strongest peaks of the later are denoted by vertical arrows); (c) the thermal evolution ($T < T_m$) of the magnetic patterns relative to the one at 4.2K.

mode within a wide range covering $-0.4 < h < 0.6$, $-0.4 < k < 0.4$, and $-0.3 < l < 0.3$. Some weak reflections were observed. Fig. 9 shows the thermal evolution of one of these peaks and, for comparison, also that of the (0,0,4) peak. As evident, the intensity of the (0,0,4) peak, being due to magnetic and nuclear contributions, decrease smoothly and goes to the value of the nuclear intensity as the temperature reaches T_c . In particular there is no visible variation in the (0,0,4) intensity when T is varied across T_m , indicating that the event at this temperature, does not belong to the main phase. On the other hand, the intensity of the other peak decays very fast as the temperature increases and is almost within the

TABLE I: Comparison of the space groups, atomic positions, and isotropic thermal parameters of TbCo₂B₂C and TbNi₂B₂C. The data on TbNi₂B₂C are taken from Lynn *et al.*⁶ The same thermal parameters reported for TbNi₂B₂C are also used for the analysis of TbCo₂B₂C.

		Tb	Co	B	C	
TbNi ₂ B ₂ C	<i>P4/mmm</i>	position	(000)	($\frac{1}{2}$ 0 $\frac{1}{4}$)	(0,0,0.357)	($\frac{1}{2}$ $\frac{1}{2}$ 0)
		thermal factor	0.47	0.57	0.77	0.85
TbCo ₂ B ₂ C	<i>Immm</i>	position	(000)	($\frac{1}{2}$ 0 $\frac{1}{4}$)	(0,0,0.354)	($\frac{1}{2}$ $\frac{1}{2}$ 0)
		thermal factor	0.47	0.57	0.77	0.85

experimental uncertainty when $T > 2$ K. Such a thermal evolution is similar to the features observed in the magnetization hysteresis (Fig. 1), in the specific heat anomaly (inset of Fig. 3), and in the powder neutron diffractograms (Figs. 5-7). This suggests that this, as well as the other weak peaks, are related to the same impurity phase as discussed above. Evidently, the ratio of the intensity of this contaminating peak to that of the (0,0,4) peak is extremely small in the single-crystal sample; in terms of the above mentioned impurity scenario, this means that the impurity concentration in the single-crystal sample is much smaller than the one in the polycrystalline case: this conclusion is supported by the observation that the intensity of the specific heat event at T_m is hardly evident in the single-crystal sample (see the inset of Fig. 3).

Based on the above conclusions, the powder diffractograms below T_m were analyzed, with the Rietveld method, as a superposition of three patterns: the nuclear, the FM mode, and a third unidentified contaminating magnetic phase. The Rietveld analysis of the nuclear and magnetic patterns of the main phase below T_m is straightforward and gave a satisfactorily fit; the diffractograms are shown in Fig. 7 while the obtained structural and magnetic parameters are given in Fig. 8; the latter figure reveal that the lattice parameters evolve smoothly across T_m and, furthermore, the mismatch parameter $(a - b)/a$ is the same as the one manifested in the magnetostriction experiment of Fig. 4 (a). On the other hand, Fig. 8 (c) compares the reduced Tb magnetic moment, $\mu(T)/\mu(2 \text{ K})$, with the calculated Brillouin function, $B_6(x)$. The total angular momentum quantum number is taken to be 6, representing that of a free Tb³⁺ ion. Since, as shown above, there are considerable CEF effects, then this $B_6(x)$ curve should be taken as a lower bound; nonetheless, the overall thermal

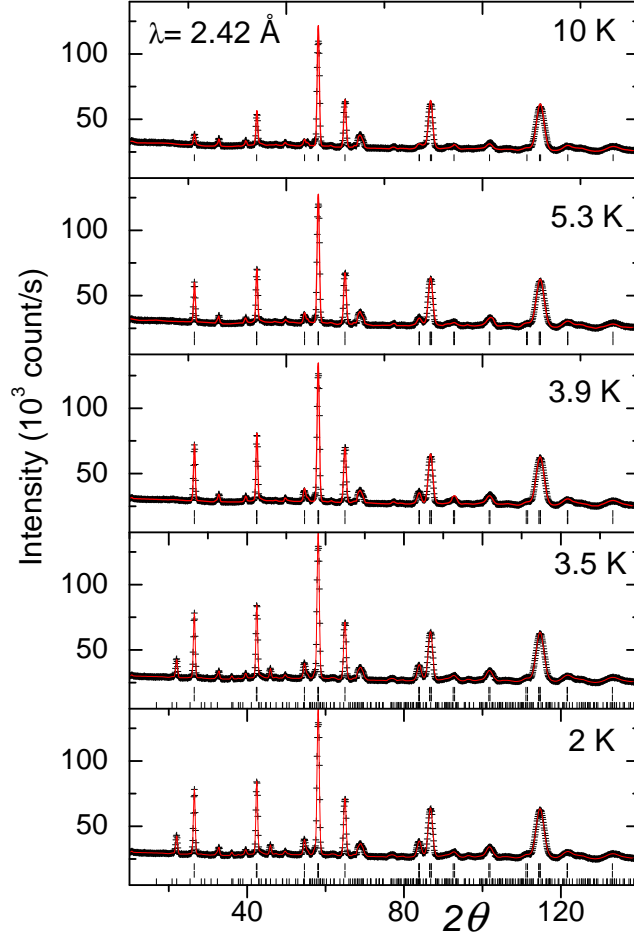


FIG. 7: (Color online) Rietveld analysis on representative powder diffractograms. Within the range $T_m < T < T_c$, the total contribution is composed of a nuclear and a FM component while for $T < T_m$ it is a sum of three phases: a nuclear, a FM, and an impurity phase (see text). The thermal evolution of the lattice parameters and magnetic moment are given in Fig. 8. The Bragg R -factor for the structural phase clusters around 2 while for the magnetic phase around 2.1.

evolution of $\mu(T)/\mu(2\text{ K})$ follows reasonably well this $B_6(x)$ curve; in particular, it reveals a smooth and monotonic evolution across the T_m region. Finally, the intensity contribution of the unidentified phase was calculated using the so-called profile matching³⁷ (or pattern decomposition) procedure. Since the crystal structure parameters of this unidentified phase are unknown, no significance should be attached to the fit of the impurity phase, only that all the additional weak peaks are associated with the impurity phase and that the presence of this phase would not modify the conclusions reached about the magnetic properties of the $\text{TbCo}_2\text{B}_2\text{C}$ phase.

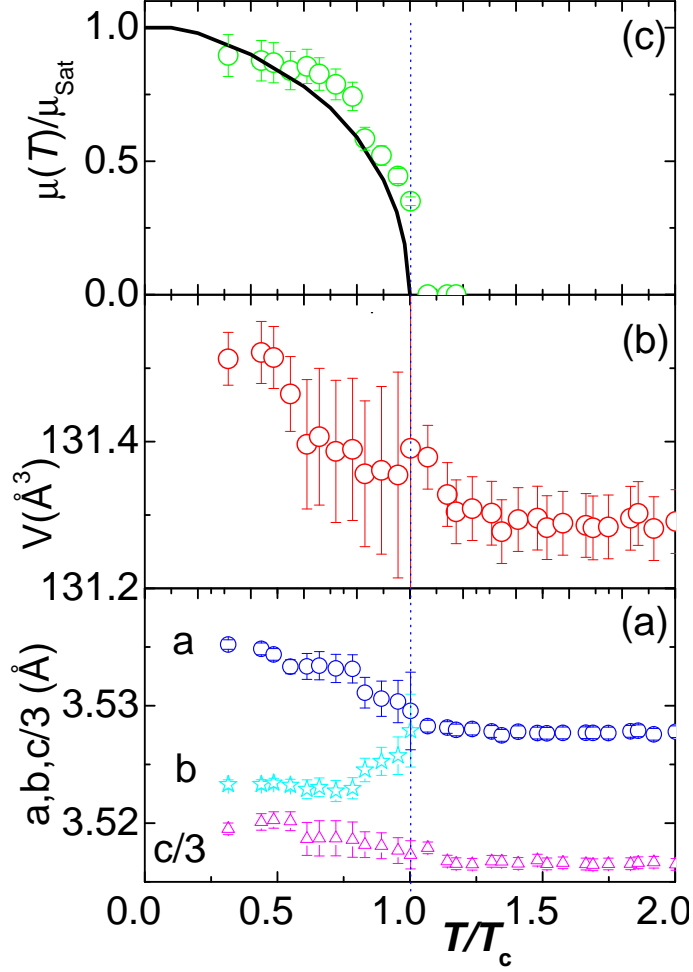


FIG. 8: (Color on line) The lattice parameters (a - b) and the reduced magnetic moment $\mu(T)/\mu(2\text{ K})$ versus the reduced temperature T/T_c (c). These parameters were obtained from the Rietveld analysis (see Fig. 7). The solid line in the upper panel represent the Brillouin function for $J=6$.

IV. DISCUSSION AND CONCLUSIONS

The above results show that the paramagnetic susceptibilities are given by the CW behavior of the Tb^{3+} moments, that this contribution is strong enough to mask any magnetic contribution of Co-sublattice (if there is any), that μ_{eff} and μ_{sat} are typical of Tb^{3+} ion and are almost equal to the ones observed in $\text{TbNi}_2\text{B}_2\text{C}$ (see Table II), and that the transition at T_c is identified as being due to the FM order of the Tb sublattice. In addition, the sample-dependent T_m -event is associated with magnetic contamination. Below we give a further argument in support of this latter identification. Obviously, if such a T_m -event is

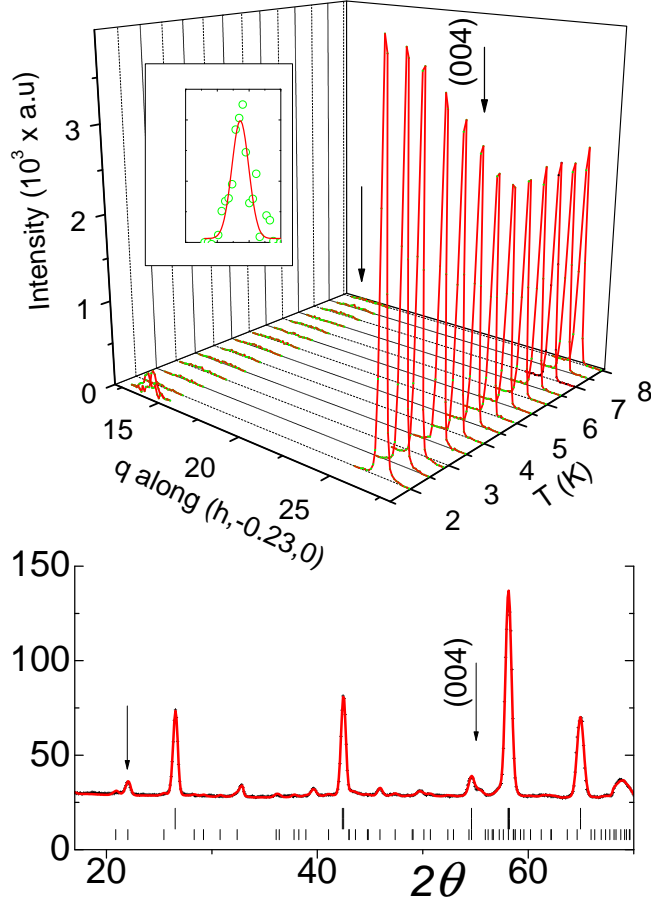


FIG. 9: The upper panel shows, on a three dimensional plot, the thermal evolution of the (0,0,4) peak and an impurity peak. The latter together with its Gaussian fit is shown, on an expanded scale, in the inset. The lower panel shows the powder diffractogram at 2 K (taken from Fig.7). The intensity of the (0,0,4) and impurity peaks (marked by a vertical arrow) are almost equal in the powder diffractogram but are a factor of 20 different in the single-crystal diffractograms (no correction for multiplicity factors are considered). The wave length used for the measurement in the upper panel is 2.3606 \AA while for the lower panel is 2.42 \AA .

intrinsic, then it must be either due to the Co- or Tb- sublattice. That the $M(H, T < T_C)$ and $^{100}\lambda_{100}(H, T < T_C)$ isotherms do not show any metamagnetic transition and that the same FM state of Tb sublattice is being maintained across T_m , then this T_m -event can not be related to a rearrangement (in direction or strength) of the Tb FM sublattice.

Let us now discuss the claim that the Co orbitals which, being on the verge of ferromagnetism, are spontaneously polarized. But the fulfilment of this possibility requires that

$H_{\text{eff}}^{\text{Co}} \geq H_{\text{cr}}^{\text{Co}}$, a relation which can, *a priori*, be satisfied since $H_{\text{eff}}^{\text{Co}}$ increases monotonically as T decreases [see Fig. 8 (c)]. In this case, there should be two magnetic transitions: one related to the R -subsystem and another to the Co-subsystem; just as in the case of, e.g., $\text{Er}_{0.6}\text{Y}_{0.4}\text{Co}_2$.³⁸ Then, as observed in other intermetallics,^{1,2,3,4} such induced Co-moments should couple ferrimagnetically with the Tb^{3+} FM sublattice. As there are no spontaneous or field-induced metamagnetic transitions in the $M(H, T < T_C)$ curves, then the possibility of a spontaneously polarized Co moment must be excluded; as such $H_{\text{eff}}^{\text{Co}} < H_{\text{cr}}^{\text{Co}}$ (see § III.A).

TABLE II: A comparison of the lattice and magnetic parameters of the isomorphous $\text{TbCo}_2\text{B}_2\text{C}$ and $\text{TbNi}_2\text{B}_2\text{C}$. The lattice parameters are reported for samples at LHe temperatures except the c parameter of $\text{TbNi}_2\text{B}_2\text{C}$; the later was estimated by normalizing its room temperature value using the values of $\text{HoNi}_2\text{B}_2\text{C}$.⁶

	$a(\text{Å})$	$b(\text{Å})$	$c(\text{Å})$	$\mu_{\text{eff}}(\mu_B)$	$T_{C,N}(\text{K})$	Magnetic Mode	$\mu_{\text{sp}}(\mu_B)$
$\text{TbCo}_2\text{B}_2\text{C}$	3.535	3.523	10.560	9.7	6.3	FM $q=(000)$	7.6
$\text{TbNi}_2\text{B}_2\text{C}$	3.554 ^a	3.534 ^a	10.44 ^b	9.8 ^c	15 ^c	LSW, $q=(0.45,0,0)$ ^b	7.78 ^{b,c}
^a Ref. ³⁵ ,			^b Ref. ⁶ ,			^c Ref. ²⁶	

It is significant that the FM structure of $\text{TbCo}_2\text{B}_2\text{C}$ is drastically different from any of the reported magnetic structures of borocarbides,⁶ in particular $\text{TbNi}_2\text{B}_2\text{C}$ even though these Tb-based isomorphs are similar in most (if not all) of the single-ion CEF-influenced properties such as the anisotropy, the strength, and the orientation of Tb moments (see § III.A and D). However, these isomorphs are distinctly different (see Table II) in the value of their transition points, in their magnetic structures, and in the overall features of their $H - T$ phase diagrams (a simple one-boundary FM phase versus a cascade of field-induced phase transitions). These differences suggest that the effective Tb-Tb magnetic couplings must be different and, furthermore, those nesting features²¹ that are responsible for the modulated mode in $\text{TbNi}_2\text{B}_2\text{C}$ must be absent in $\text{TbCo}_2\text{B}_2\text{C}$. These differences, prompted by the introduction of the Co atoms, suggest that the configuration of their electronic structures [in particular the position of E_F within the $N(E)$ curve and the generalized susceptibilities] must be different. As mentioned in § I, these arguments are consistent with the findings of the electronic structure calculation on $\text{LuCo}_2\text{B}_2\text{C}$:²⁰ these calculations provide an explanation for the surge of the enhanced paramagnetic character of $\text{YCo}_2\text{B}_2\text{C}$ and the

absence of superconductivity in any of the $R\text{Co}_2\text{B}_2\text{C}$ compounds (even though $\text{YCo}_2\text{B}_2\text{C}$ has the same Debye and Sommerfeld coefficients as $\text{YNi}_2\text{B}_2\text{C}$).^{19,24}

Finally, it is recalled that the indirect exchange coupling in metallic magnets are usually written as:³⁹

$$J(R_{ni}) = \frac{9\pi n^2 \Gamma^2 (g-1)^2}{8V^2 E_F} F(2k_F R_{ni}) \exp(-R_{ni}/\lambda),$$

$$F(x) = \left[\frac{x \cos(x) - \sin(x)}{(x)^4} \right],$$

where Γ is the $s-f$ exchange coupling, n is the carrier concentration [governed by $N(E_F)$], R_{ni} is the distance separating the moments, E_F and k_F are the Fermi energy and wave vector, and $\lambda (> R)$ is the mean free path. Considering that these couplings manifest a quadratic dependence on $N(E_F)$ and a sensitive sinusoidal dependence on the moments separating distances, then it is no surprise that the combination of difference in the electronic structure²⁰ and in the lattice parameters (see Table I) would lead to strong variation in the magnitude and sign of the coupling constants and as such to drastic difference in the magnetic structures of these Tb-based isomorphs. In fact this difference is not limited to these Tb-based isomorphs, our preliminary studies on the magnetic structures of the $R\text{Co}_2\text{B}_2\text{C}$ series showed that this is valid for the whole $R\text{Co}_2\text{B}_2\text{C}$ magnets:⁴⁰ as an example, the FM mode is observed in $\text{TmCo}_2\text{B}_2\text{C}$ and $\text{HoCo}_2\text{B}_2\text{C}$.

Acknowledgments

We acknowledge the partial financial support from the Brazilian agencies CNPq (485058/2006-5) and Faperj (E-26/171.343/2005).

-
- ¹ D. Bloch and R. Lemaire, Phys. Rev. B **2**, 2648 (1970).
 - ² D. Bloch, D. M. Edwards, M. Shimizu, and J. Voiron, J. Phys. F: Metal Phys. **5**, 1217 (1975).
 - ³ M. Cyrot and M. Lavagna, J. Phys. (Paris) **40**, 763 (1979).
 - ⁴ M. Cyrot, D. Gignoux, F. Givourd, and M. Lavagna, J. Phys. (Paris) **40**, C5 (1979).
 - ⁵ K.-H. Müller and V. N. Narozhnyi, Rep. Prog. Phys. **64**, 943 (2001).
 - ⁶ J. W. Lynn, S. Skanthakumar, Q. Huang, S. K. Sinha, Z. Hossain, L. C. Gupta, R. Nagarajan, and C. Godart, Phys. Rev. B **55**, 6584 (1997).

- ⁷ A. J. Campbell, D. McK. Paul, and G. J. McIntyre, Phys. Rev. B **61**, 5872 (2000).
- ⁸ P. Dervenagas, J. Zarestky, C. Stassis, A. I. Goldman, P. C. Canfield, and B. K. Cho, Physica B **212**, 1 (1995).
- ⁹ L. J. Chang, C. V. Tomy, D. M. Paul, and C. Ritter, Phys. Rev. B **54**, 9031 (1996).
- ¹⁰ A. B. Sternlieb, C. Stassis, A. I. Goldman, P. Canfield, and S. Shapiro, J. Appl. Phys. **81**, 4938 (1997).
- ¹¹ S. K. Sinha, J. W. Lynn, T. E. Grigereit, Z. Hossain, L. C. Gupta, R. Nagarajan, and C. Godart, Phys. Rev. B **51**, R681 (1995).
- ¹² J. Zarestky, C. Stassis, A. I. Goldman, P. C. Canfield, P. Dervenagas, B. K. Cho, , and D. C. Johnston, Phys. Rev. B **51**, R678 (1995).
- ¹³ P. Dervenagas, J. Zarestky, C. Stassis, A. I. Goldman, P. C. Canfield, and B. K. Cho, Phys. Rev. B **53**, 8506 (1996).
- ¹⁴ C. Detlefs, D. L. Abernathy, G. Grubel, and P. C. Canfield, Europhys. Lett. **47**, 352 (1999).
- ¹⁵ P. C. Canfield, S. L. Bud'ko, and B. K. Cho, Physica C **262**, 249 (1996).
- ¹⁶ C. Detlefs, C. Song, S. Brown, P. Thompson, A. Kreyssig, S. L. Budko, , and P. C. Canfield, cond-mat/0306742 (30-Jun-2003).
- ¹⁷ H. Kawano-Furukawa, H. Takeshita, M. Ochiai, T. Nagata, H. Yoshizawa, N. Furukawa, H. Takeya, and K. Kadowaki, Phys. Rev. B **65**, 180508(R) (2002).
- ¹⁸ S.-M. Choi, J. W. Lynn, D. Lopez, P. L. Gammel, P. C. Canfield, and S. L. Bud'ko, Phys. Rev. Lett. **87**, 107001 (2001).
- ¹⁹ M. El Massalami, H. A. Borges, H. Takeya, R. E. Rapp, and A. Chaves, J. Magn. Magn. Mater. **279**, 5 (2004).
- ²⁰ R. Coehoorn, Physica C **228**, 331 (1994).
- ²¹ J. I. Lee and et al, Phys. Rev. B **50**, 4030 (1994).
- ²² L. F. Matthias, Phys. Rev. B **49**, 13279 (1994).
- ²³ W. E. Pickett and D. J. Singh, Phys. Rev. Lett **72**, 3702 (1994).
- ²⁴ M. ElMassalami, M. S. DaCosta, R. E. Rapp, and F. A. B. Chaves, Phys. Rev. B **62**, 8942 (2000).
- ²⁵ M. El Massalami, E. F. Chagas, and R. E. Rapp, J. Magn. Magn. Mater **226-230**, 1058 (2001).
- ²⁶ B. K. Cho, P. C. Canfield, and D. C. Johnston, Phys. Rev. B **53**, 8499 (1996).
- ²⁷ C. V. Tomy, L. A. Afalfiz, M. R. Lees, J. M. Martin, D. McK Paul, and D. T. Adroja, Phys.

- Rev. B **53**, 307 (1996).
- ²⁸ A. Kreyssig, O. Stockert, A. Dreyhaupt, E. Ressouche, B. G. C. Ritter, H. Bitterlich, G. Behr, P. C. Canfield, and M. Loewenhaupt, *J. Low Temp. Phys.* **131**, 1129 (2003).
- ²⁹ C. Song, D. Wermeille, A. I. Goldman, P. C. Canfield, J. Y. Rhee, and B. N. Harmon, *Phys. Rev. B* **63**, 104 507 (2001).
- ³⁰ H. Takeya, E. Habuta, H. Kawano-Furukawa, T. Ooba, and K. Hirata, *J. Magn. Magn. Mater.* **226**, 269 (2001).
- ³¹ M. ElMassalami, M. Amara, R.-M. Galera, D. Schmitt, and H. Takeya, *Phys. Rev. B* **76**, 104410 (2007).
- ³² X. B. Liu and Z. Altounian, *J. Phys.: Condens. Matter* **18**, 5503 (2006).
- ³³ J. Herrero-Albillos, F. Bartolomé, L. M. García, A. T. Young, T. Funk, J. Campo, and G. J. Cuello, *Phys. Rev. B* **76**, 094409 (2007).
- ³⁴ M. Kruis, G. R. Pickett, and M. C. Veuro, *Phys. Rev. B* **177**, 910 (1969).
- ³⁵ C. Song, Z. Islam, L. Lottermoser, A. I. Goldman, P. C. Canfield, and C. Detlefs, *Phys. Rev. B* **60**, 6223 (1999).
- ³⁶ C. Song, J. C. Lang, C. Detlefs, A. Letoublon, W. Good, J. Kim, D. Wermeille, S. L. Bud'ko, P. C. Canfield, and A. I. Goldman, *Phys. Rev. B* **64**, 20 403 (2001).
- ³⁷ J. Rodríguez-Carvajal, *Physica B* **192**, 55 (1993).
- ³⁸ R. Hauser, E. Bauer, E. Gratz, H. Müller, M. Rotter, H. Michor, G. Hilscher, A. Markosyan, K. Kamishima, and T. Goto, *Phys. Rev. B* **61**, 1198 (2000).
- ³⁹ B. Coqblin, *The Electronic Structure of Rare-Earth Metals and Alloys: The Magnetic Heavy Rare-Earth* (Academic Press, New York, 1977).
- ⁴⁰ M. ElMassalami et al, to be Published.
- ⁴¹ C. Kittel, *Quantum Theory of Solids* (John Wiley and Sons Inc., New York, 1963).

APPENDIX A: MAGNON CONTRIBUTION FROM THE FERROMAGNETIC TB-SUBLATTICE OF $\text{TBCO}_2\text{B}_2\text{C}$

The above-mentioned ferromagnetic order of the Tb-sublattice suggests that the dominant exchange interactions within the same layer (approximated by a positive J_1) as well as those among different layers (approximated by a positive J_2) are ferromagnetic. Let us assume

that the main contributions to the magnetic energy is due to the above-mentioned exchange couplings and anisotropic crystalline electric field interactions. Within the low temperature regime of interest, the anisotropic interactions can be approximated by an effective field \vec{H}_a (in energy units) which, for this particular case, forces the moments to points along the a axis. The Hamiltonian (under zero external field) can be written as:

$$\mathcal{H} = - \sum_{i,j \in A,B} J_1 \vec{S}_i \cdot \vec{S}_j - \sum_{\langle ij \rangle, i \in A, j \in B} J_2 \vec{S}_i \cdot \vec{S}_j - \vec{H}_a \cdot \sum_{i \in A,B} \vec{S}_i \quad (\text{A1})$$

All symbols have their usual meanings. The first term sums the bilinear products of two neighboring spins of the the same layer A and afterwards the contribution of all layers are added together. The second term sums all the bilinear product of two neighboring spins (each belong to a different but an adjacent layer). The third term is a sum over all single-ion anisotropic energies. Using standard linear spin-wave approximation (considering a non-interacting magnon gas), Eq. A1 can be diagonalize to give the following dispersion relation:

$$\begin{aligned} \hbar\omega_k = & SJ_1(4 - 2 \cos bk_x - 2 \cos ak_z) + \\ & 2SJ_2 \left\{ \begin{aligned} & 4 - \cos(\frac{a}{2}k_z + \frac{b}{2}k_x + \frac{c}{2}k_y) - \cos(-\frac{a}{2}k_z + \frac{b}{2}k_x + \frac{c}{2}k_y) - \\ & - \cos(\frac{a}{2}k_z - \frac{b}{2}k_x + \frac{c}{2}k_y) - \cos(\frac{a}{2}k_z + \frac{b}{2}k_x - \frac{c}{2}k_y) \end{aligned} \right\} + H_a, \end{aligned}$$

where z (the quantization axis), x, y axes are, respectively, along the a (easy direction), b, c directions of the crystallographic unit cell. In the long wave limit, up to second order, this simplifies to:

$$\hbar\omega_k = \Delta + c_x k_x^2 + c_y k_y^2 + c_z k_z^2. \quad (\text{A2})$$

Assuming a weaker orthorhombic distortion ($a \approx b$ and $c_x \approx c_z$), one gets:

$$c_x = Sa^2(J_1 + J_2) \equiv c_z$$

$$c_y = Sc^2 J_2.$$

The energy gap ($k = 0$) is:

$$\Delta = H_a \quad (\text{A3})$$

The expression for the density of states (obtained from integrating over the constant energy surface, $\epsilon \equiv \omega$) is:

$$\rho(\epsilon) = \frac{V}{(2\pi)^3} \int \frac{dS_\epsilon}{|\nabla \hbar\omega_k|} = \frac{V}{2\pi^2} \frac{\sqrt{\epsilon - \Delta}}{c_x \sqrt{c_y} a^2 c}. \quad (\text{A4})$$

The magnon contribution to the total energy is:

$$E = E_0 + \int_{\Delta}^{\infty} d\epsilon \frac{\epsilon \rho(\epsilon)}{e^{\beta\epsilon} - 1}$$

where E_0 is a constant independent of temperature. Using Eqs. A2, A3, and A4, the molar specific heat is (ν is the number of moles):

$$C_{mag}(T) = \frac{1}{\nu} \frac{dE}{dT} = \frac{R}{2\pi^2 c_x \sqrt{c_y}} \frac{1}{T^2} \sum_{n=1}^{\infty} I_n,$$

where

$$I_n = n \int_{\Delta}^{\infty} d\epsilon \epsilon^2 \sqrt{\epsilon - \Delta} e^{-n\beta\epsilon} = 2ne^{-n\beta\Delta} \left\{ \frac{1.3.5.\sqrt{\pi}}{2^4(n\beta)^{7/2}} + 2\Delta \frac{1.3.\sqrt{\pi}}{2^3(n\beta)^{5/2}} + \Delta^2 \frac{\sqrt{\pi}}{2^2(n\beta)^{3/2}} \right\}.$$

The final result can be rearranged to give:

$$C_{mag}(T) = \frac{15.R\Delta^{\frac{3}{2}}}{8.\pi^{\frac{3}{2}}D^{\frac{3}{2}}} \sum_{n=1}^{\infty} n. \exp\left(-\frac{n\Delta}{T}\right) \left[\frac{4}{15} \left(\frac{T}{n\Delta}\right)^{-\frac{1}{2}} + \left(\frac{T}{n\Delta}\right)^{\frac{1}{2}} + \left(\frac{T}{n\Delta}\right)^{\frac{3}{2}} \right] \quad (\text{A5})$$

where

$$D = 2^{\frac{1}{3}} S (J_1 + J_2)^{\frac{2}{3}} J_2^{\frac{1}{3}} \quad (\text{A6})$$

is the spin-wave stiffness coefficient⁴¹ which is a measure of the effective coupling strength. This expression reproduces the high temperature limit ($T \gg \Delta$),

$$C_M(T) \propto e^{-\Delta/T} T^{3/2},$$

which for $\Delta = 0$ gives the well known $\frac{3}{2}$ -Bloch expression.⁴¹ At lower temperatures ($T \ll \Delta$), the strong dependence on the gap is emphasized by the expression:

$$C_M(T) \propto e^{-\Delta/T} T^{-1/2}.$$